GEORG-AUGUST UNIVERSITÄT GÖTTINGEN

BACHELOR THESIS

Scaling Exponents in One-Dimensional Breath Figures

Skalenexponenten für Tropfen auf einem Faden

prepared by

Philipp Dönges

from Northeim

at the Institute for Nonlinear Dynamics

Contents

1 Introduction

1.1 Motivation

Vapor condensing on surfaces forms a pattern called *breath figure* composed of a multitude of droplets [9]. These patterns are frequently encountered in daily life, for example the dew on leaves in the morning or the fogged mirror in the bathroom after taking a shower. On a transparent cooking lids one can nicely observe the dynamics: New droplets arise at free spots and slowly grow by absorption of steam. When two droplets get too close to each other they merge and release space, where new droplets emerge.

Breath figures are also common in technical applications, for instance in fog harvesting [4, 7], cooling processes based on condensation [11] and filter systems [13].

1.2 Phenomenology of Breath Figures

When talking about breath figures, we call D the dimension of the droplets and d the dimension of the surface the droplets are condensing on. In physically relevant cases of cause $D = 3$, and the dimension of the substrate can be either $d = 1$ as in case of a spiderwebs or $d = 2$ as in the example of a mirror. In any case one has $D > d$.

The development of the breath figure is driven by a flux of mass Φ on the surface. Usually we assume this flux to be constant in time and space. The water condensing on areas already covered by a droplet cause the droplet to grow, the water condensing on free areas drives the nucleation of new droplets. The D-dimensional size of a droplet is called s, the smallest possible size of a droplet is s_0.

If two droplets A and B get too close to each other they merge and form another larger droplet C. Upon merging the volume is conserved, $s_C = s_A + s_B$, while the covered area shrinks, as $s_C^{\frac{d}{D}} < s_A^{\frac{d}{D}} + s_B^{\frac{d}{D}}$ for $d < D$. Consequently each merging event provides new free area, on which new small droplets will originate.

At late times merges of very large droplet release very large free areas. On these areas the whole droplet developing process will start all over again, reminiscent of a new breath figure starting to develop on a blank surface. Consequently, breath figures feature fractal, self-similar droplet distributions.

The temporal development of one-dimensional breath figures can be nicely visualized in space-time plots. One can use the vertical axis of the plot for the time and mark

3

areas covered by a droplet on the horizontal axis. In figure 1 this is shown with a color code referring to the size of the droplets.
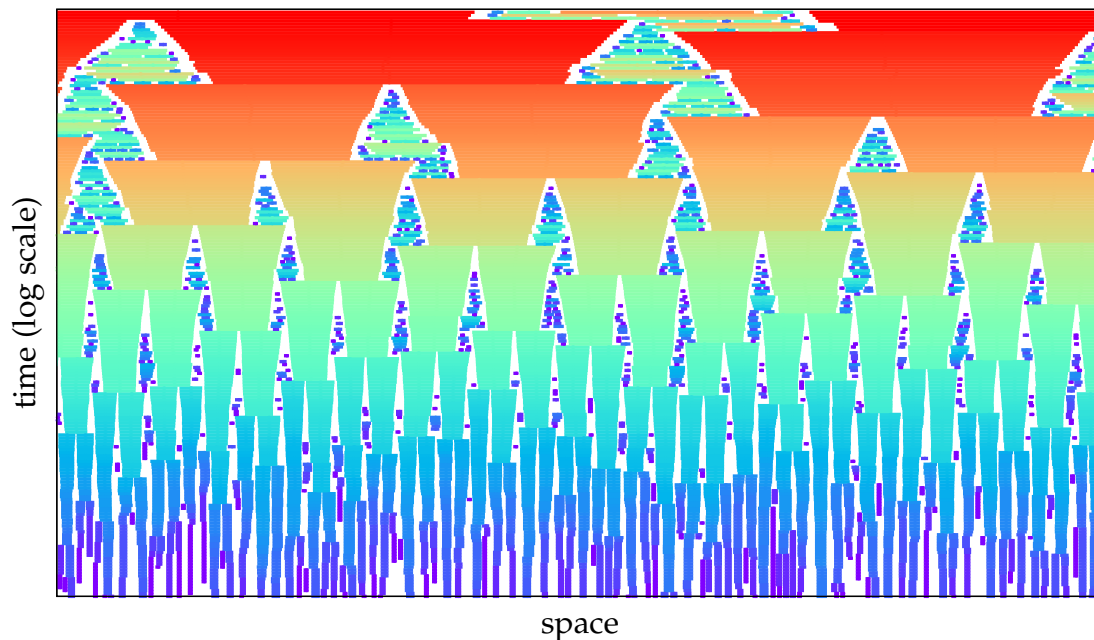
Figure 1: *Space-time plot of the evolution of the simulation of a one-dimensional breath figure (confer section 1.3 for a description of the model). The colored area is covered by droplets, where the color refers to the size of the considered droplet. The plot is based on data provided by Klös [6].*

One can distinguish different growth regimes of breath figures, the scaling theory considered in this work only describes the regime in which the breath figure is self-similar. It is easy to see in the space-time plot in figure 1, that at early times there are only new, small droplets. It takes some time until the droplets have grown to a size when they can release sufficiently large free areas by merging, on which new droplets can arise. In experiments there is also an additional regime later on in which the droplets are deformed by gravity, a situation which is not described by the scaling theory. There is no gravitation in the simulations and thus the simulation data gets closer and closer to a perfect scaling regime at late time.

1.3 Dynamics in Numerical Simulation

When starting my bachelor thesis there already was a huge amount of simulation data for one-dimensional breath figures. They were calculated by Gunnar Klös during his

bachelor thesis [6] based on a program written in C by Jürgen Vollmer. All data analysis presented in the present work refers to this data.

In this simulation a constant flux of mass on the one-dimensional surface is achieved by adding one droplet of the smallest possible size in each time step. After each addition of a droplet the program checks, whether the new droplet is too close to or even inside an already existing droplet. In that case the new droplet instantly merges with the older one. If a droplet is added in a small gap between two droplets such that it overlaps with both ones, it merges with the one to which surface the distance is smaller. When merging the droplet volumes are added, the center of the new droplet is calculated as the center of mass of both merging droplets. It is possible that one merging event causes another one, in that case two merging events occur in one time step.

The evolution of the system in the simulation is documented by regularly writing the centers and volumes of all droplets to a file. The time steps for the output follow a logarithmic scaling, because the largest droplets at late times change less per unit time.

1.4 Experiment

In addition to the analysis of the simulation data I have contributed to build an experimental system of a one-dimensional breath figure. The basic idea of this experiment was first described by Klös [6] and is shown in figure 2. It is based on a setup for two-dimensional breath figures. The setup is composed of four horizontal glass plates, bordered in an aluminum housing. The glass plates define three chambers, the outer ones are flooded by hot water for temperature control, the inner one is used as test chamber. In this chamber we place a thread that serves as a quasi-one-dimensional surface to be populated by the breath figure. A thin layer of water on the bottom of the middle chamber provides humid air in the chamber, which leads to water condensing on the thread. The developing breath figure can be observed by illumination from below and taking pictures from above.

Although conceptually this looks like a straight forward experiment, it is hard to find a suitable thread, i.e. a suitable quasi-one-dimensional surface. It needs to be both as thin and hygroscopic as possible. We considered using a cooled metal wire with high heat conductivity, an empty glass fiber carrying cooling liquid, a spider thread and a grove in the upper glass plate. Presently the glass fiber appears to be the most promising approach.
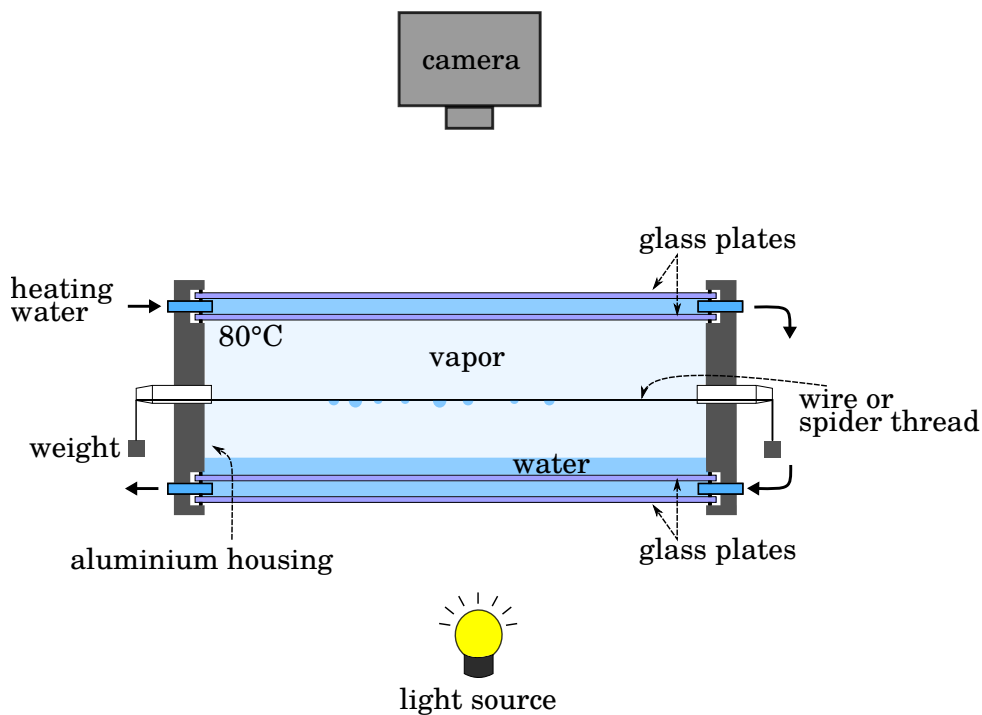
Figure 2: *Sketch of a setup to observe one-dimensional breath figures, obtained from [6].*

The fibers used in our experiment were manufactured by Marcin Makowski a postdoctoral student at the MPIDS. They have a diameter of about 100 microns, and as cooling liquid we use water with a temperature only slightly above the freezing point. The temperature of the heating water, the aluminum housing and the humid air are kept to a temperature of about 60 to 65 degrees. With this setup it is possible to achieve condensation, droplet formation and droplet merging on the glass fiber that are reminiscent to the evolution of breath figures in an early state of developing. Unfortunately we do not yet reach the late stage self-similar regime, as needed to determine the non-trivial exponent important in the scaling theory and introduced in chapter 2.

1.5 Outline

The present work will contribute on the discussion about a non-trivial exponent in the theory describing breath figures in the self-similar regime.
We first revisit the classical scaling theory in chapter 2 and show the necessity and meaning of the non-trivial exponent. In the first part of chapter 3 we present theoretical considerations to estimate values for this exponent. The second part of the chapter is about determining the exponent in simulation data. The main finding of that section

will be, that extreme care is needed to avoid misinterpreting the data. In chapter 4, I take a closer look on the gaps between the droplets and I summarize the main result and discuss the open issues in chapter 5

2 Scaling Theory of Breath Figures

The following theory describes the droplet distribution and its development in breath figures in the self-similar regime. Breath figures entered the physical literature in a heated debate of Rayleigh and Aitken in the early 20th century [9]. The analysis of their scaling properties was first explored by Viovy, Beysens & Knobler [1] and Family & Meakin [5] around 1990.

2.1 Droplet Size Distributions

We consider D-dimensional droplets condensing onto a d-dimensional surface with a constant flux of mass Φ. Let $n(s,t)$ be the number of droplets with D-dimensional size s in the system at time t. Thereby the time t is dimensionless, measured by the time needed to place one of the smallest droplets on each length of their diameter on the surface. As illustrated in figure 3 the size dependence of this droplet distribution fulfills a power law with exponent θ. The different curves for different times are all of the same shape, except for a shift reflecting the droplet growth. Hence, we assume that the time evolution only depends on the ratio of droplet size to the size Σ of the largest droplets. In practice there also is a minimal possible size of droplets, so we introduce a lower cutoff function $\hat{g}(s)$ being equal to 1 for large enough values, and zero for very small ones. Thus we assume

$$n(s,t) = s^{-\theta} \cdot f\left(\frac{s}{\Sigma(t)}\right) \cdot \hat{g}(s). \tag{1}$$

The exponent θ is easily determined by dimension analysis: n has the unit $1/[\text{length}]^{D+d}$, s the unit $[\text{length}]^D$, and f and $\hat{g}$ are dimensionless. Hence, the exponent θ is found to be

$$\theta = \frac{d+D}{D}. \tag{2}$$

The time evolution of the droplet distribution is conveniently determined by following the largest droplets. To characterize their evolution, we explore first how they grow as a function of the total volume of all droplets.
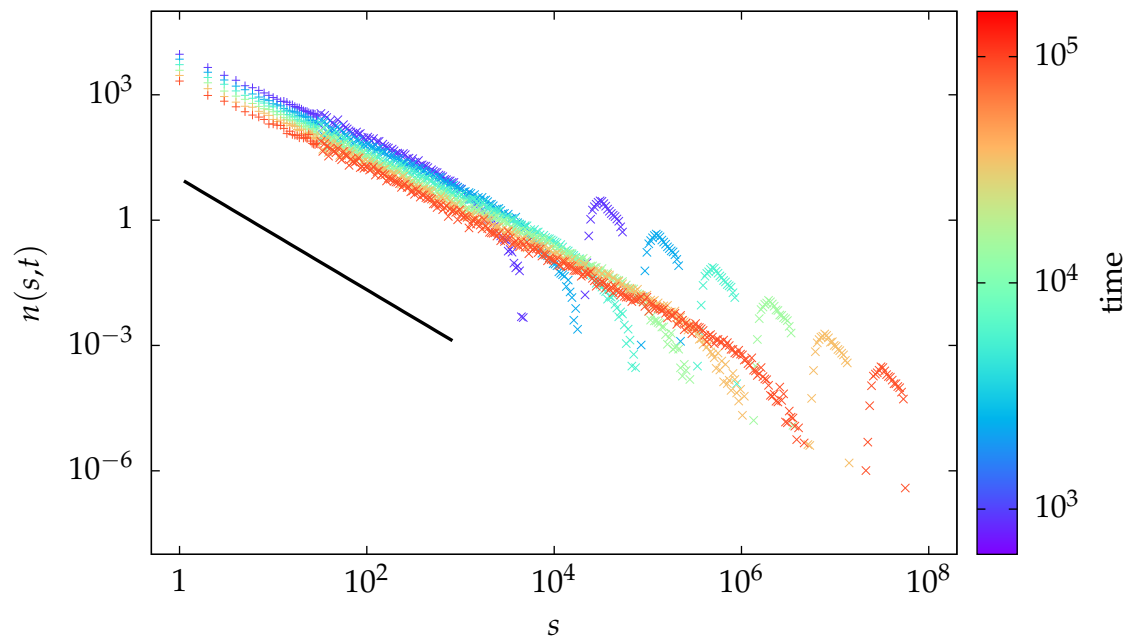
Figure 3: *The number of droplets as function of droplet size and time. For s < 30 the data point are linearly binned (marked by +), and for larger droplets we use a logarithmic binning (marked by ×). The solid line shows a power law ∼ s^{−θ} with θ = 4/3.*

2.2 Total Volume

The total volume V of all droplets is linearly increasing in time due to a constant flux of mass Φ. The resulting total volume is the sum over all droplet volumes. In the continuum limit for many droplets it is defined as the integral:

$$\Phi t = V = \int_0^\infty sn(s,t)\,ds \tag{3}$$
$$= \int_0^\infty s^{1-\theta} f\left(\frac{s}{\Sigma(t)}\right) \hat{g}(s)\,ds.$$

The lower cutoff function $\hat{g}$ can be replaced by a lower bound of integration s_V:

$$\Phi t = V = \int_{s_V}^\infty s^{1-\theta} f\left(\frac{s}{\Sigma(t)}\right)\,ds$$
$$= \int_{s_V/\Sigma}^\infty (\Sigma \cdot x)^{1-\theta} f(x)\,\Sigma\,dx, \qquad\qquad x = s/\Sigma$$
$$= \Sigma^{2-\theta} \int_{s_V/\Sigma}^\infty x^{1-\theta} f(x)\,dx$$
$$\overset{\text{large }\Sigma}{=} c_V\,\Sigma^{1-\frac{d}{D}} = c_V\,R^{D-d}, \qquad\qquad R = \Sigma^{-D}. \tag{4}$$

The value of the constant c_V can be estimated by considering a system of droplets of equal size and distances as sketched in figure 4. Let $\{t_n\}$ be the moments, in which all droplets are touching both neighbors, and let R_n be the radius of the droplets at time t_n. As always two droplets merge in each time step one has $R_{n+1} = 2R_n$. For $d = 1$ one can use the relation (4) to calculate the ratio of two consecutive time steps:

$$\frac{t_{n+1}}{t_n} = \frac{R_{n+1}^{D-d}}{R_n^{D-d}} = \left(\frac{2R_n}{R_n}\right)^{D-1} = 2^{D-d}. \tag{5}$$

The volume ΔV added to the system of length $4R_n$ in the time between t_n and t_{n+1} can be considered with different approaches. On the one hand it is the volume difference between two droplets with radius R_n and one with radius R_{n+1}:

$$\Delta V = R_{n+1}{}^D - 2R_n{}^D = (2^D - 2)\,R_n{}^D = 2R_n\left(2^{D-d} - 1\right) R^{D-d}. \tag{6}$$

On the other hand one can think of it as the volume deposited on the system in the

time between t_n and t_{n+1} by the flux Φ:

$$\Delta V = 4R_n \, \Phi \, (t_{n+1} - t_n) = 4 \, R_n \, \Phi \, (2^{D-1} - 1) \, t_n. \tag{7}$$

For $d = 1$ combining this two relations leads to

$$R_n{}^{D-1} = 2 \, \Phi \, t_n. \tag{8}$$

Comparing to relation (4) yields

$$c_V = \frac{1}{2} \Rightarrow \Sigma = (2\Phi t)^{\frac{3}{2}} \, . \tag{9}$$
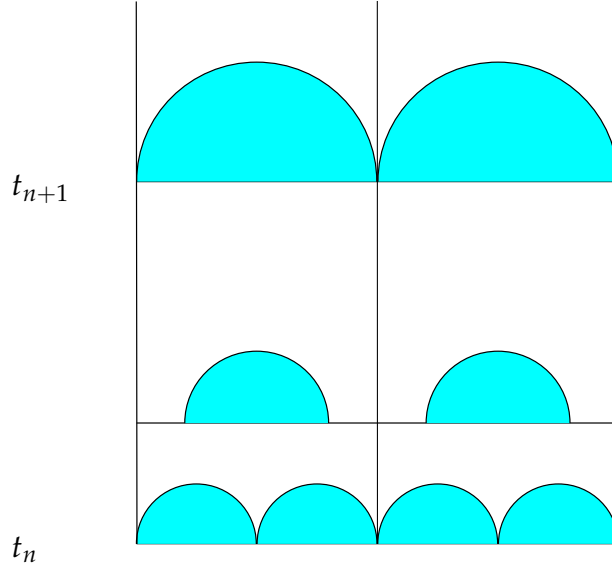
Figure 4: *Sketch of droplet merging.*

With that in mind one can rescale the droplet size distribution, and plot $s^\theta n(s,t)$ as function of s/Σ (see figure 5). In that way we get a closer look at the function f. Once again a power law can be observed; f can be written as product of an exponential term $(s/\Sigma)^{\theta-\tau}$ and a cutoff function $\hat{f}(s/\Sigma)$ which includes a dip and a bump. Thus, one has

$$n(s,t) = s^{-\theta} \left(\frac{s}{\Sigma}\right)^{\theta-\tau} \hat{f}\left(\frac{s}{\Sigma}\right) \hat{g}(s). \tag{10}$$

The exponent τ is nontrivial as far as there are only few guesses in the literature [2],

while different values have been encountered for measurements in experiments and simulations. In order to gain insight into the physical content of this exponent we consider the evolution of the porosity of breath figures.
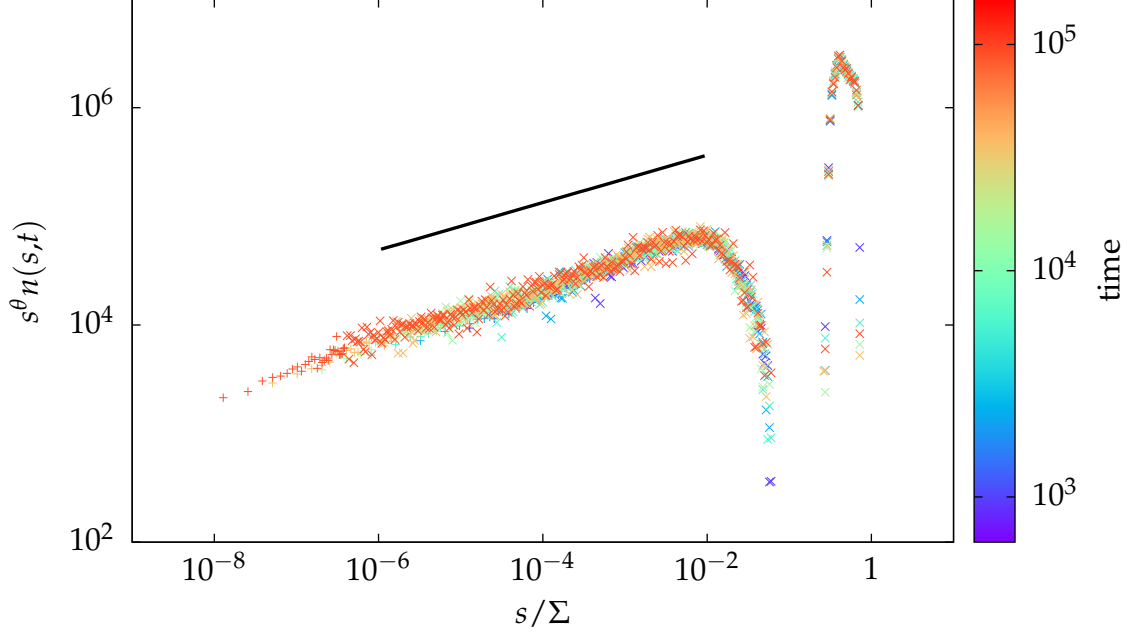
Figure 5: *A master plot of all the droplet distributions displayed in figure 3 is obtained by rescaling based on the relations (9) and (10).*

2.3 Porosity

We denote the total length covered by droplets as A, and determine the porosity $1 - A$, i.e. the total length of all gaps between droplets. The covered length can be calculated as an integral over the length of each droplet:

$$1 - A = 1 - \int_0^\infty s^{\frac{d}{D}} \, n(s,t) \, \mathrm{d}s \tag{11}$$
$$= 1 - \int_0^\infty x^{\theta - \tau - 1} \, \hat{f}(x) \, \hat{g}(s) \, \mathrm{d}x, \qquad x = s/\Sigma.$$

When there is no lower cutoff of the droplet size, the whole length is covered:

$$1 = \int_0^\infty x^{\theta - \tau - 1} \, \hat{f}(x) \, \mathrm{d}x. \tag{12}$$

Thus, equation (11) can be rewritten as

$$1 - A = \int_0^\infty x^{\theta - \tau - 1} \hat{f}(x) \, dx - \int_0^\infty x^{\theta - \tau - 1} \hat{f}(x) \, \hat{g}(s) \, dx$$

$$= \int_0^\infty x^{\theta - \tau - 1} \hat{f}(x) \, [1 - \hat{g}(s)] \, dx \tag{13}$$

As $\hat{g}$ is the lower cutoff function, $1 - \hat{g}$ is an upper cutoff function. It is equal to one for small values of s and zero for large droplets. Therefore, the influence of the upper cutoff function $\hat{f}$ reduces for fully developed breath figure to the constant value $\hat{f}_0$ for small sizes. As the remaining integral is finite, we can replace the unknown function $\hat{g}$ by a step function with the step at the point s_A, whereby the value s_A is choose such that the considered integral remain the same:

$$1 - A = \hat{f}_0 \, \Sigma^{\tau - \theta} \int_0^{s_A} s^{\theta - \tau - 1} \, ds$$

$$= \frac{\hat{f}_0}{\theta - \tau} \left(\frac{s_A}{\Sigma} \right)^{\theta - \tau} \sim t^{\frac{3}{2}(\tau - \theta)}. \tag{14}$$

As shown in figure 6 this long term behavior is nicely observable in data. One can determine the non-trivial exponent τ by a careful measurement of the porosity in experiments or simulations.

The theoretical calculation of the porosity confirms the necessity of the dependence $n(s,t) \sim \left(\frac{s}{\Sigma} \right)^{\theta - \tau}$. For $\tau = \theta$ the integral in equation (13) and hence the porosity diverges logarithmically. Consequently the porosity would be unbounded, while it clearly must be smaller than 1 by definition.

The need for a non-trivial exponent $\theta - \tau$ is also apparent in the total number of droplets.
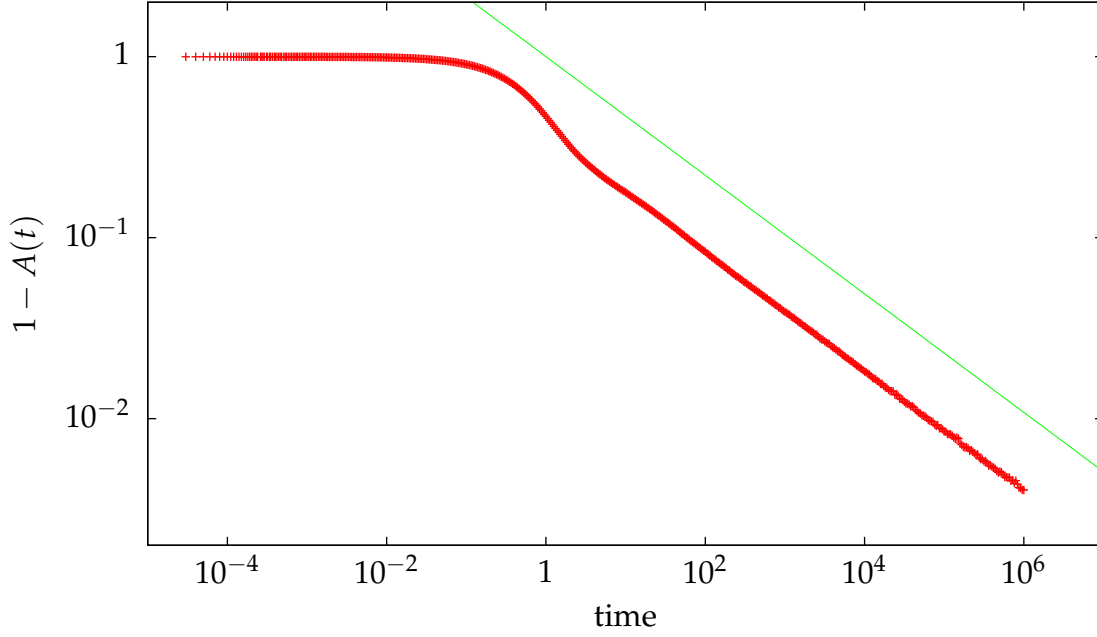
Figure 6: *The Porosity as function of the normalized time.*

2.4 Total Number of Droplets

The time evolution of the total number of droplets, $N(t)$, is obtained as

$$
\begin{aligned}
N &= \int_0^\infty n(s,t)\, \mathrm{d}s \\
&= \int_0^\infty s^{-\theta} \left(\frac{s}{\Sigma}\right)^{\theta-\tau} \hat{f}\left(\frac{s}{\Sigma}\right) \hat{g}(s)\, \mathrm{d}s \\
&= \Sigma^{1-\theta} \int_{s_N/\Sigma}^\infty x^{-\tau} \hat{f}(x)\, \mathrm{d}x \\
&= \Sigma^{1-\theta} \hat{f}_0 \left[c_N - \frac{1}{1-\tau} \left(\frac{s_N}{\Sigma}\right)^{1-\tau}\right] \\
&= \frac{\hat{f}_0}{(\tau-1)\, s_N{}^{\theta-1}} \left(\frac{s_N}{\Sigma}\right)^{\theta-\tau} \left[1 + (\tau-1)\, c_N \left(\frac{s_N}{\Sigma}\right)^{\tau-1}\right] \\
&\stackrel{\text{large }\Sigma}{=\joinrel=} \frac{\hat{f}_0}{(\tau-1)\, s_N{}^{\theta-1}} \left(\frac{s_N}{\Sigma}\right)^{\theta-\tau}.
\end{aligned}
$$

Thus, the asymptotic behavior for large values of Σ is equal to the behavior of the porosity. However, the convergence is very slow due to the second term. One should rather use the porosity to determine τ.

14

Once again the calculation shows the need of the non-trivial exponent. In the trivial case $\tau = \theta$ the total number of droplets is found to be $N = \text{const} + \text{h.o.t.}$. However, this is impossible when the droplets grow in size.

2.5 Interaction Radius

In experiments two droplets can merge even before they touch each other due to an additional interaction range of each droplet. There are two different approaches to implement this interaction range in simulations: One can set a constant interaction radius for each droplet as observed for spherical droplets in experiment, or one can set the interaction radius of each droplet proportional to its radius as observed for barrel-shaped droplets. It has been shown [6] that an interaction proportional to the droplet radius can trivially be incorporated into the definition of droplet size. Therefore, I concentrate in the following on a constant interactions radius. The rescaled droplet distributions for some representative interaction radii are plotted in figure 7.
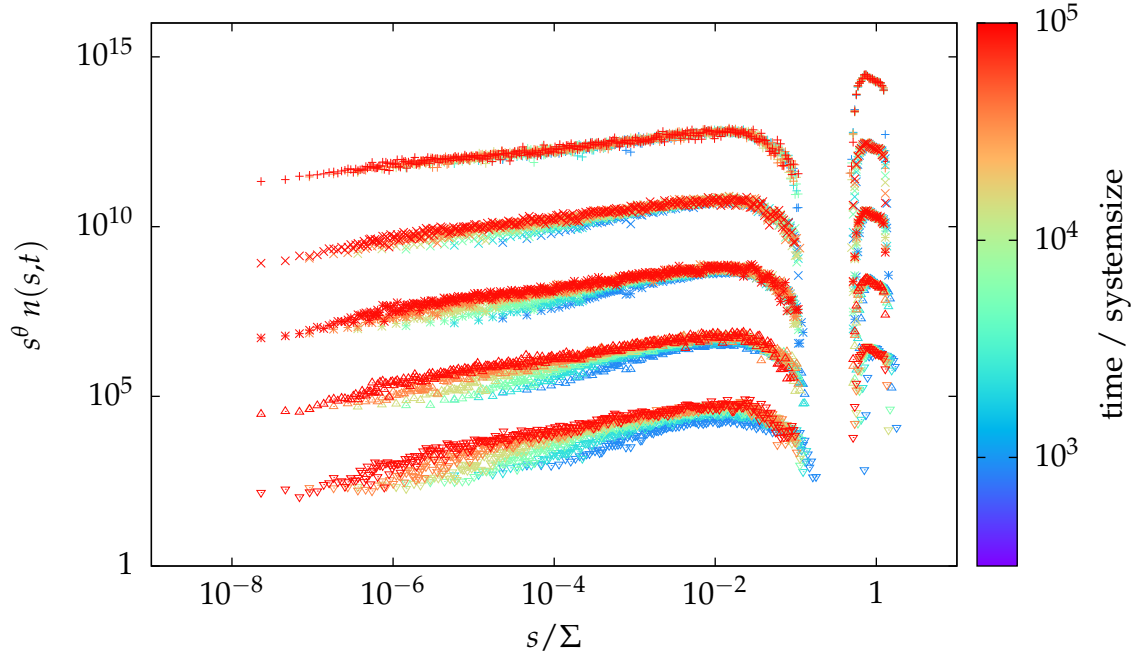
Figure 7: *The rescaled droplet distributions for different constant interaction radii of (from top to bottom) 0, 1, 2, 4 and 8. For better comparison we shifted the curves: The bottom curve is not shifted, the other curves are each shifted up by two decades as compared to the one below.*

3 The Non-Trivial Exponent

As seen above there is a non-trivial exponent τ appearing in the formula (10) for the droplet distribution and thus in the whole scaling theory. In this section we will take a closer look at theoretical and numerical estimates for the value of τ.

3.1 Theoretical Approaches

3.1.1 Blackman

In 2000 Blackman et al. [2] used renormalisation group theory to calculate an explicit value for τ. In the calculation he assumed, that the probability kernel for the coalescence of two droplets of the sizes s_A and s_B factorizes in the probabilities to find each droplet independent. In other words he assumed that the sizes of neighboring droplets are uncorrelated, a statement which is not true [8], but a possible simplification. The calculation provides a prediction for τ. In our case, for $D = 3$ and $d = 1$, they predict

$$\tau_B = \frac{5d - 3}{4D} + 1 = \frac{1}{2D} + 1 = \frac{7}{6}. \tag{15}$$

3.1.2 Own Considerations

For one-dimensional breath figures the same value can also be in a more transparent way. Let us consider a section of length L in a one-dimension breath figure. We only consider droplets with a size larger than a value s_c. and we require s_c to be large enough, that we can ignore the lower cutoff function in the following. Due to this choice the lower limit for droplets entering the expression for the porosity. Equation (13) slightly changes in

$$p(\Sigma) = 1 - \int_{s_c}^{\infty} s^{\frac{1}{D}} \, n(s, \Sigma(t)) \, \mathrm{d}s$$

$$= \frac{\hat{f}_0}{\theta - \tau} \left(\frac{s_c}{\Sigma} \right). \tag{16}$$

In the self-similar regime, the considered section should feature the same appearance after scaling it up by a factor $a > 1$. The only difference is the missing of all droplets

between s_c and as_c. The number of these missing droplets can be calculated as

$$\Delta N_a(\Sigma) = \Sigma^{1-\theta} \int_{s_c/\Sigma}^{a^D s_c/\Sigma} x^{-\tau} \hat{f}(x) \, \mathrm{d}x$$

$$= s_c^{1-\theta} \frac{\hat{f}_0}{\tau - 1} \left(\frac{s_c}{\Sigma}\right)^{\theta - \tau} \left(1 - a^{D(\tau-1)}\right). \tag{17}$$

After adding these droplets the porosity should be the same again. Thus we obtain

$$aL \, p(a^D \Sigma) = aL \, p(\Sigma) - aL \, s_c^{\frac{1}{D}} \, \Delta N_a(\Sigma)$$

$$\Rightarrow 1 - a^{D(\theta - \tau)} = \frac{\theta - \tau}{\tau - 1} \left(1 - a^{-D(\tau-1)}\right). \tag{18}$$

As this argumentation should work for all $a > 1$. Hence, equation (18) requires that $\theta - \tau = \tau - 1$. the result only applies to $d = 1$ such that we find

$$\tau = \frac{d}{2D} + 1, \tag{19}$$

in full agreement with Blackman's result, equation (15), when evaluated for $d = 1$.

3.2 Determination in Simulation Data

As suggested in section 2.3 I determine τ by fitting the decay of the porosity.

3.2.1 Basic Fit

A plot of the time evolution of the porosity for different interaction radii is shown in figure 8. Interestingly the values of τ determined in this basic fit depend on the interaction radius. As shown in figure 9 they grow from 1.115 to 1.13 when the interaction radius increase from 0 to 24. A clear trend is observed, with errorbars small as compared to the changes. This is surprising, because the theory predicts a constant value for τ, independent of microphysical details like interaction radii. Furthermore, all of the determined values of τ are far away from the value $\tau_B = 1.1\bar{6}$ predicted in equation (15).

In order to analyze this remarkable IR-dependence we take a closer look on the underlaying fitting process. Dividing the data by the fitted function leads to the reduced plots shown in figure 10. In this representation one can see, that the functions do not
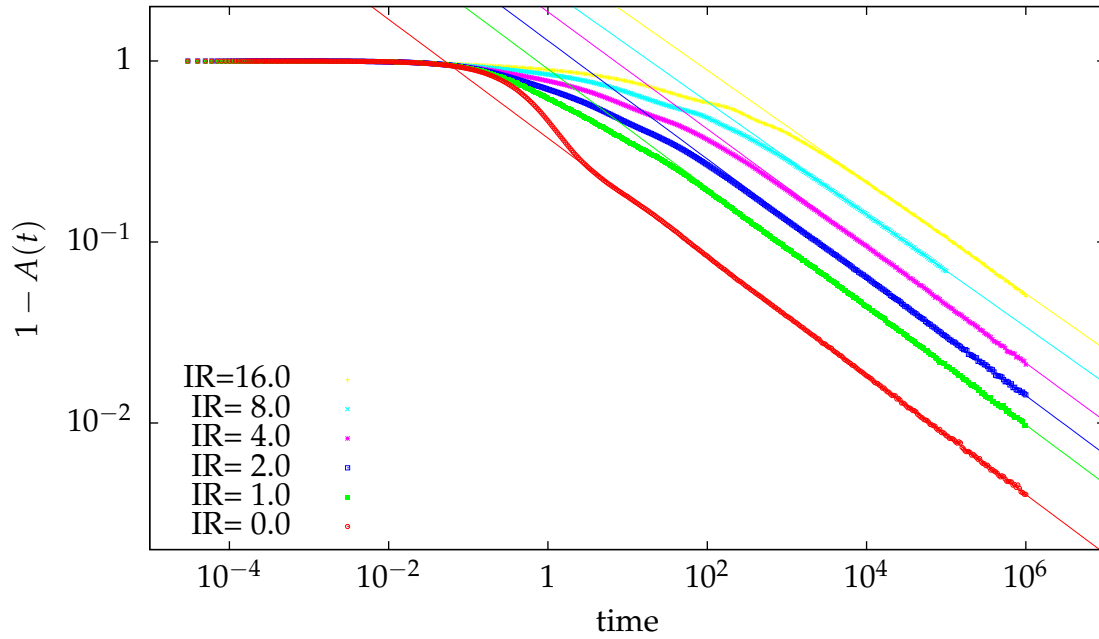
Figure 8: *The porosity for different interaction radii IR (as provided in the legend), and the related fits based on fitting the data points for $t > 10^3$.*
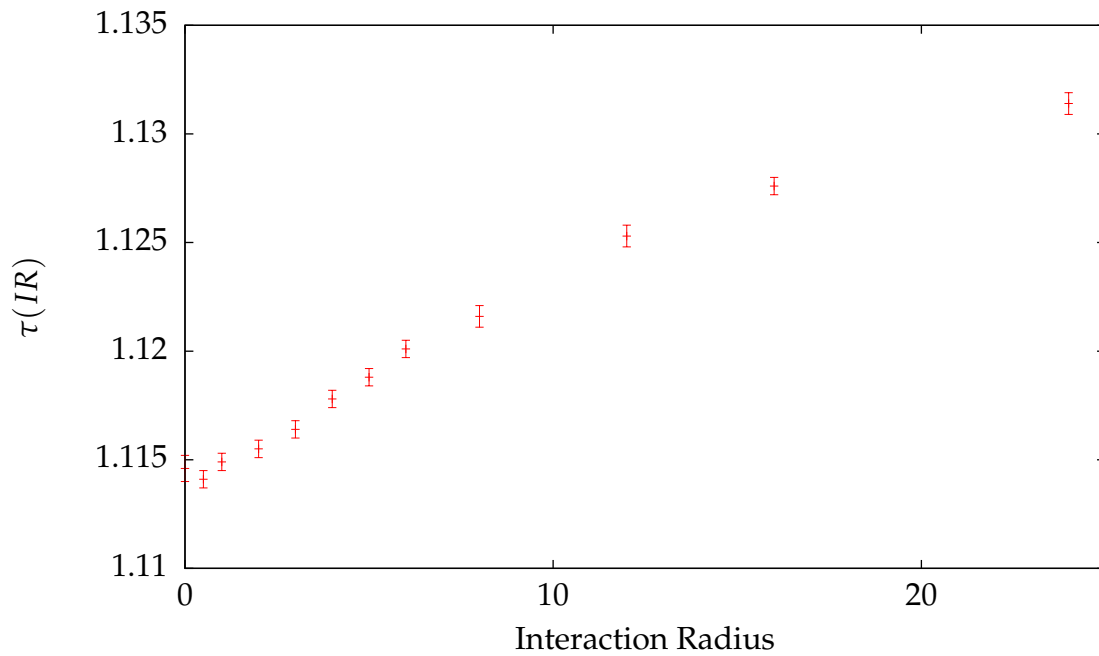
Figure 9: *The IR-dependence of τ as observed by Klös. [6]*

18

fit the data as well as they suggested by figure 8. In the range used for the fitting the data points are all sitting on a curve below the fitted function in the left and right side of the domain, and above in the middle. This observation suggests, that the transient of the porosity toward the asymptotic function is still relevant for the time values as large as $t = 10^4$. Thus, fitting of the data in the interval between 10^3 and 10^6 does not determine the asymptotic value of τ were are looking for.
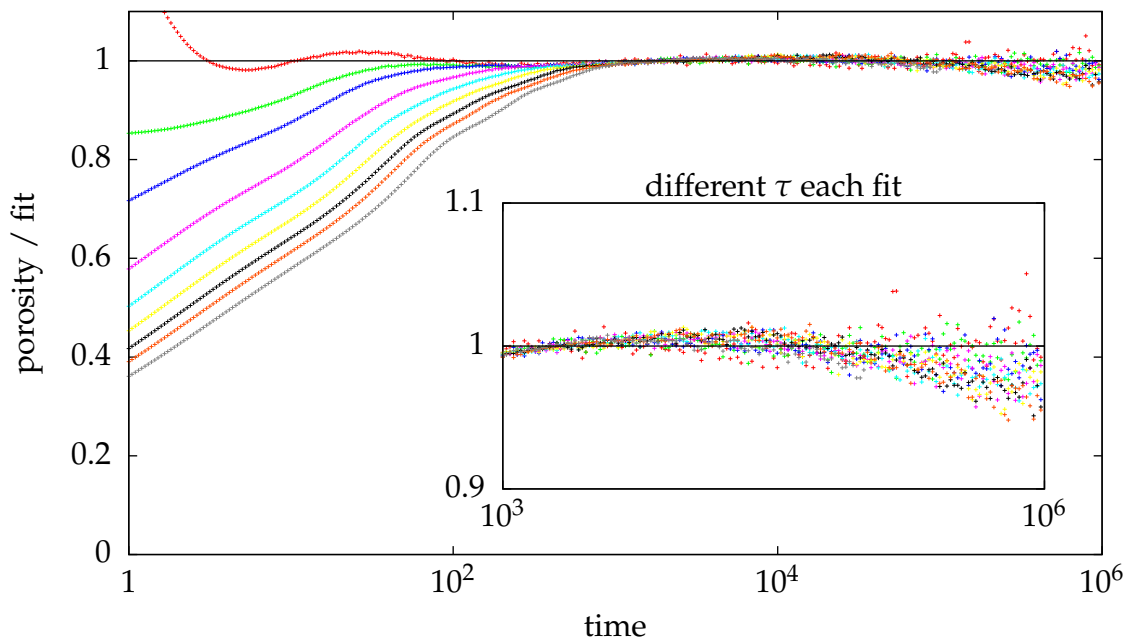
Figure 10: *Reduced plots of the fits of the porosity decay obtained in figure 8. For $t > 10^5$ the data points systematically lie below the fit. This curvature suggests, that we are fitting in a regime, where the transient towards the asymptotic value is still important.*

3.2.2 More Informed Fit

To prevent this problem and to get values closer to the asymptotic value we only fit the data for the latest times. Fitting in the interval between 10^5 and 10^6 leads to the plots shown in figure 11. In this reduced plot the predicted fitting function looks like an asymptotic that function all data curves are converging to. Particularly, the data points are now spread uniformly around the fit throughout the fit window. This suggests, that we are now really determining the wanted asymptotic value of τ.
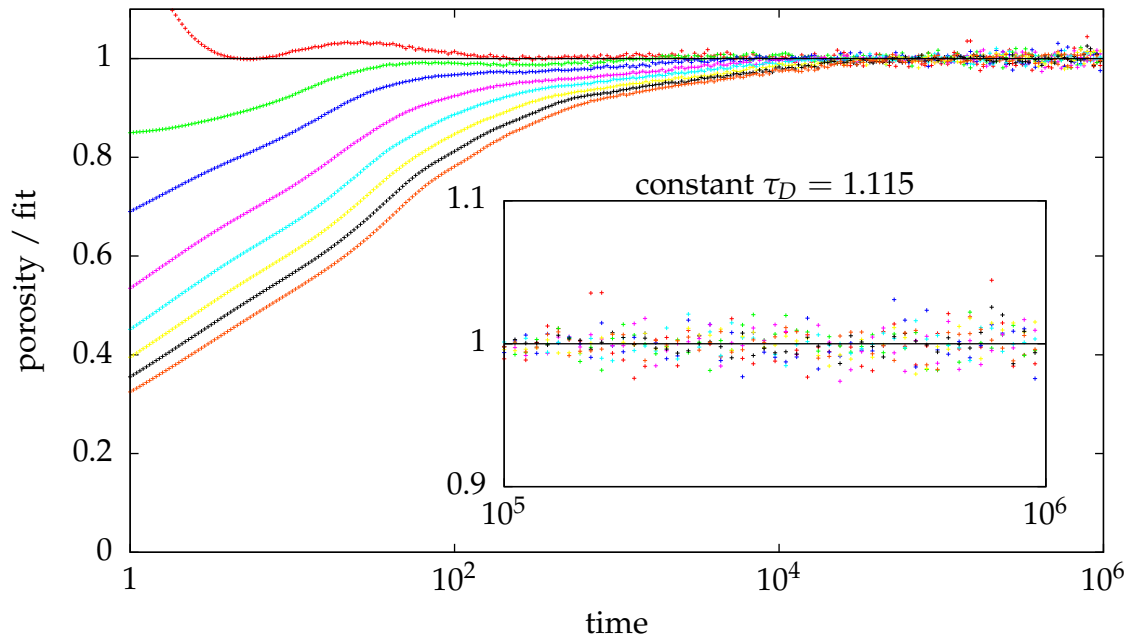
Figure 11: *Reduced plots obtained when fitting the porosity for $t > 10^5$. As one can see in the inset the data points are now spread uniformly around the fit. The fitted decay now looks like an asymptotic value that all curves slowly tend to. Interestingly within our error margins the value of τ obtained in this manner is the same for all interaction ranges, $\tau_D = 1.115$.*

Interestingly the values of τ for the different interaction radii that are obtained by the fits for $t > 10^5$ are all nearly the same, $\tau_D \approx 1.115$. This is a strong indication that τ is universal as supposed by theoretical considerations. However, we still find a value that noticeably differs from the predicted value $\tau_B = 1.1\overline{6}$.

4 Gaps

Beside the droplets we also took a look at the gaps between the droplets and their size distribution.

4.1 Gap Size Distribution

Analogously to the droplet size distribution one can consider the gap size distribution. The smallest possible droplet size is a fixed value $s_0 = 1$ by the choose of our dimensionless length. Similarly, the minimal gap size amounts to the interaction radius IR, because the two adjacent droplets merge upon approaching closer than IR, thus eliminating the gap.

The largest gaps are generated by a merge of two of the largest droplets. As the size of the largest droplets growth in time, the largest gaps are growing, too. Hence one may expect a time-dependence of the whole gap size distribution similar to the droplet size distribution. The distribution of the gap size for $IR = 5$ is plotted in figure 12.
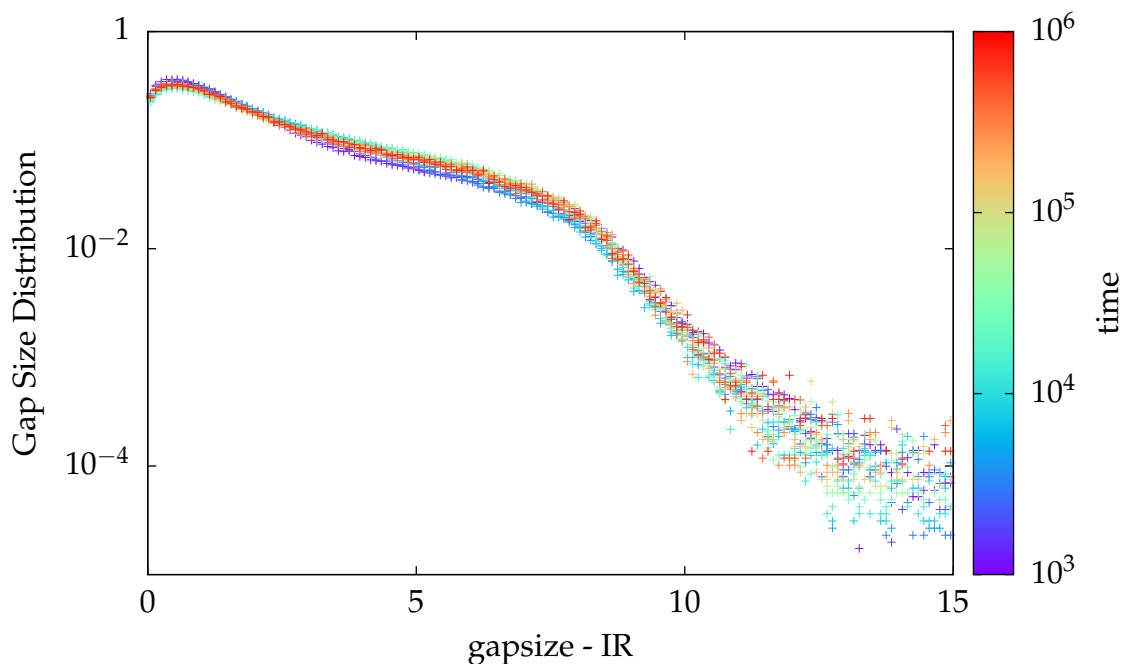
Figure 12: *Distribution of the size of the gaps for the interaction radius $IR = 5$.*

Surprisingly the gap size distribution is virtually time-independent. Certainly there

are small changes for large gap sizes, but the large gaps are extremely rare such that there is no noticeable influence on the distribution.

In contrast to the insensitivity to temporal changes of the droplet size distribution, there is a noticeable influence of the interaction radius. Even when accounting for the trivial dependence by considering the reduced gap size $g - IR$, larger interaction radii causes larger gaps, as shown in figure 13. This observation can be understood by a closer inspection of the dynamics of the mean gap size.
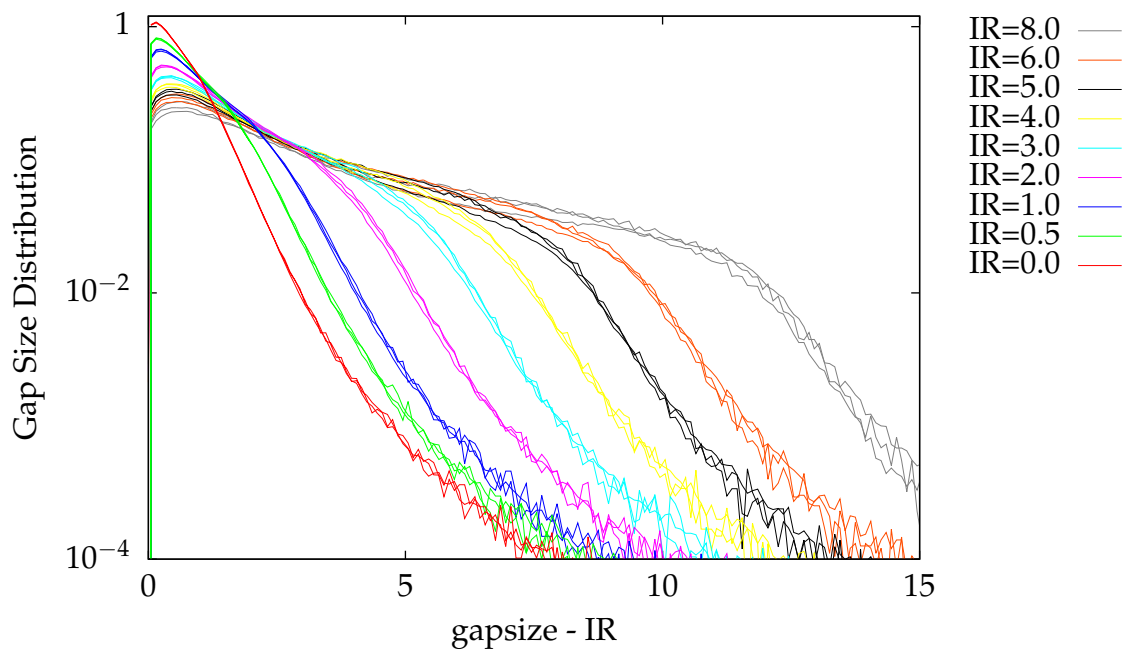
Figure 13: *Comparison of the gap size distribution for different interaction radii.*

4.2 Mean Gap Size

The mean gap size $< g >$ is calculated as the sum of all gap sizes divided by the total number of gaps. By definition the sum of all gap sizes amounts to the porosity considered in section 2.3. As each gap is bounded by two droplets and vice versa, the total number of droplets and gaps are equal in one-dimensional systems. Thus, we also know the total number of gaps from the calculations in section 2.4. Hence, we obtain

the mean gap size as

$$< g >= \frac{1 - A}{N} = \frac{\frac{\hat{f_0}}{\theta - \tau} \left(\frac{s_A}{\Sigma}\right)^{\theta - \tau}}{\frac{\hat{f_0}}{(\tau - 1) s_N^{\theta - 1}} \left(\frac{s_N}{\Sigma}\right)^{\theta - \tau} + \text{h.o.t.}}. \tag{20}$$

Neglecting the higher order therms yields

$$< g >\approx \frac{\tau - 1}{\theta - \tau} s_A^{\theta - \tau} s_N^{\tau - 1}. \tag{21}$$

Since we assumed in the calculation of both porosity and droplet number, that we are in the self-similar regime, this formula is an asymptotic function as well. Both s_A and s_N are constants describing the microphysics, thus the formula predicts, that the asymptotic value of the mean gap size is time-independent. This is in line with the finding that the gap size distribution is time invariant, and it can be directly verified by plotting the mean gap size as function of time (see figure 14). For times smaller than zero the surface is mostly empty and it is populated then by with small droplets such that the mean gap size is shrinking in this regime. Once a self-similar breath figure develops, the mean gap size tends to a constant value, that is increasing for larger IR, in line with the observation that the gap size distribution in the self-similar regime becomes broader with increasing interaction radius.

In the next section we will work out how the dependence on the interaction radius in equation (21) is hidden in s_A and s_N.

4.3 Characteristic Gap Size

The values s_A and s_N originate from the lower cutoff value while integrating over the droplet distribution to determine the porosity or the droplet number. They are barely different and both represent the size of a characteristic small droplet. Thus we assume that they are both similar to a characteristic small droplet size $s_A \sim s_N \sim s_*$. This approximation leads to

$$< g >\sim \frac{\tau - 1}{\theta - \tau} s_*^{\theta - 1}. \tag{22}$$

Since s_* is a D-dimensional droplet size and $\theta - 1 = d/D$, the expression $s_*^{\theta - 1}$ has the unit $[lenght]^d$, which correspond to a gap size.
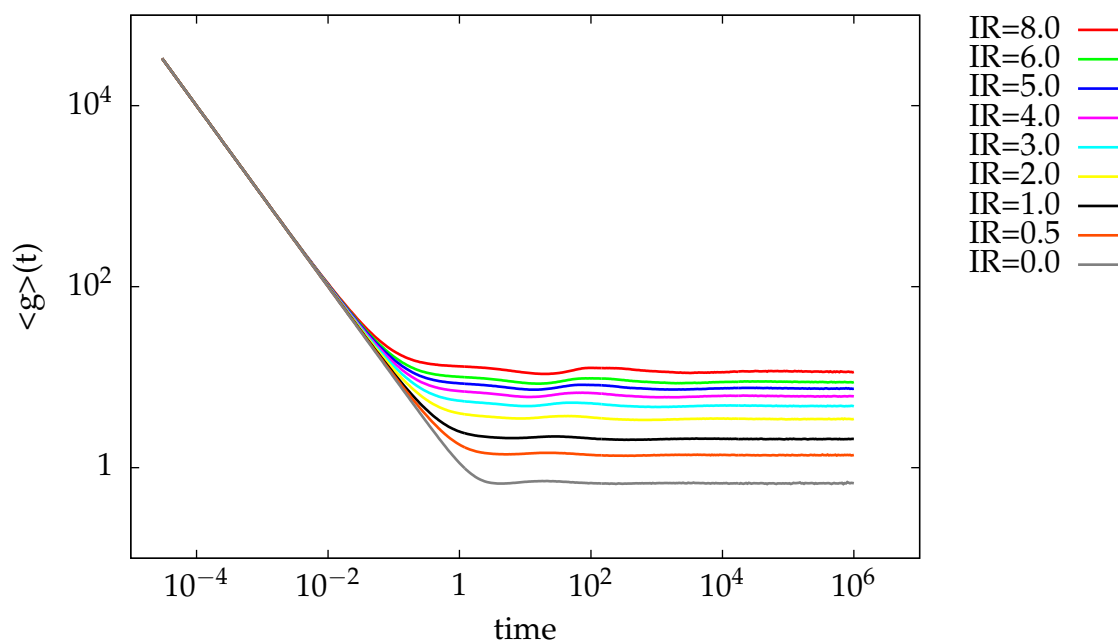
Figure 14: *Plot of the mean gap size depending on time for different interaction radii.*

The physics of gaps changes at the point, where the gaps get large enough to admit adding a new droplet. As visualized in figure 15 such a gap is of the size $1 + 2IR$. The added droplet in the middle of the old gap is of the size 1, and it must be separated by one interaction radius to both neighboring droplets. Consequently, the characteristic gap size $s_*^{\theta-1}$ should scale like $1 + 2IR$.
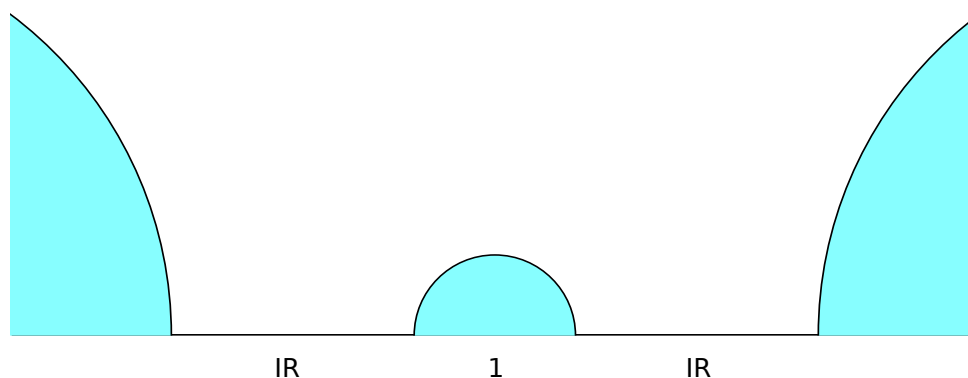
Figure 15: *Sketch of the characteristic gap size. The smallest possible gap in which a new droplet can arise is of the size $1 + 2IR$*

This statement can be checked in figure 16 by plotting the asymptotic mean gap size

as function of the interaction radius. The asymptotic values of the mean gap size are determined from 14 via fitting a constant in the last decade. Plotting them as function of the interaction radius clearly confirms the prediction $< g > \sim 1 + 2IR$. The deviation form the linear fit are shown in the reduced plot in the lower part of figure 16. The deviation from the linear dependence are of the magnitude of 2%. They clearly do not arise from statistical noise but rather point to a higher order correction to the linear approximation $L(IR)$.
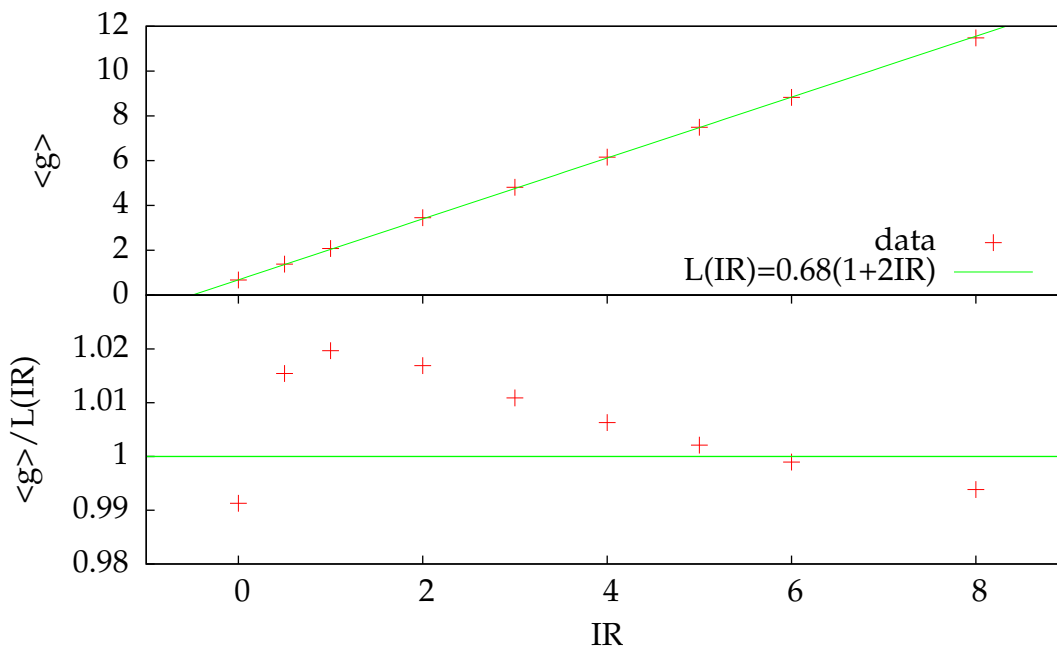
Figure 16: *The asymptotic mean gap sizes depending on the interaction radius and linear fit. The reduced plot is shown in the lower part.*

5 Conclusion

5.1 Summary

In the present work I revisited the scaling theory of breath figures and confirmed, that this theory describes our simulation data very well. To this end I examined the porosity and droplet number, and pointed out the necessity of a non-trivial exponent τ. Moreover I augmented the classical scaling theory with the estimate (9) of the size Σ of the largest droplets.

Next I considered Blackman's [2] estimation of the non-trivial exponent $\tau_B = \frac{1}{D} + 1$ for $d = 1$. For this setting I provided a new, more transparent derivation of this result.

To determine the non-trivial exponent in our simulation data I fitted the decay of the porosity. A basic fit leads to a dependence of τ on the interaction radius IR, at it was observed before by Klös [6]. However, a more careful look at the reduced plot in figure 10 shows, that the decay of the porosity is still in the transient towards an asymptotic value in spirit of the fact that the power-law data covers more than four orders of magnitude in time and more than one decade in $1 - A$.

An alternative fit in figure 11 considers this transient behavior by only fitting data in the last decade in order to determine τ. Surprisingly the IR-dependence of τ was no longer observed. Instead I found a constant $\tau_D = 1.115$.

This value is far away from the theoretical estimation $\tau_B = 1.1\bar{6}$. One possible explanation for that is, that Blackman did not consider the autocorrelation of the size of droplets, found to be not zero by Lapp [8]. I my own derivation of the theoretical value I assumed a continuous scale invariance of breath figures. However, there are indications for a discrete scale invariance, namely the oscillations of the porosity in figure 10, a typical consequence of discrete scaling [10], [12].

The multitude of different values in the literature measured in experiments and simulations, may be caused by the very long transients in observable quantities like the droplet number or the porosity. In my analysis I used data for $t = 10^6$ for my asymptotic fit, this corresponds to a ratio of largest to smallest droplet of $\Sigma/s_0 = 1000$. In experiments the transients had found to be even longer [3]. Consequently it seems to be very hard determine τ in an experiment like ours described in section 1.4, at least not via the established approaches.

While considering the gaps I observed, that their size distribution does not depend on time, but on interaction radius. I took a closer look on the asymptotic mean gap size

and found a characteristic gap size $s_* = 1 + 2IR$ both in theory, equation (22), and simulation data, figure 16, to be responsible for the IR-dependence.

5.2 Outlook

Although there are many indicators, that the non-trivial exponent τ is not universal, the researches done in the present work suggest that it is, but only in the asymptotics reached at very late times. If this statement is true, longer simulations for times beyond $t = 10^6$ should confirm it. Of cause it would be great to determine the asymptotic value of τ in experiments, too. However, this may need a new approach for a measurable quantity besides the porosity and the droplet number, as the transients of these quantities seems to be too long.

On the other hand the issue, that it is hard to reach the asymptotic regime in experiments also means, that breath figures will not reach this regime in most technical applications. Consequently, it is not sufficient to understand the asymptotics, but one also needs profound insight into the transients and the oscillations observed in the experimentally accessible regimes.

Nomenclature

Variable	Meaning
D	Dimension of the droplets
d	Dimension of the substrat
t	Time (usually dimensionless)
$s(t)$	Dropletsize (D-dimensional)
$\Sigma(t)$	Size of the largest droplets
$n(s,t)$	Number of droplets with size s
$N(t)$	Total number of droplets
Φ	Volumen flux onto the substrat
$V(t)$	Total size/volumen of droplets
θ	Trivial power exponent
τ	Nontrivial power exponent
$\hat{f}(x)$	Upper cutoff function
$\hat{g}(x)$	Lower cutoff function
$\hat{f}_0$	Asymptotic value of $\hat{f}(x)$ for small x
IR	Interaction radius
g	Gap size
$<g>$	Mean gap size
s_*	Characteristic gap size

List of Figures

References

[1]   Daniel Beysens et al. "Growth of a droplet pattern (Breath figures) on a surface". In: *Dynamics of Ordering Processes in Condensed Matter*. Springer, 1988, pp. 403–413.

[2]   JA Blackman and S Brochard. "Polydispersity exponent in homogeneous droplet growth". In: *Physical Review Letters* 84.19 (2000), p. 4409.

[3]   Johannes Blaschke et al. "Breath Figures: Nucleation, Growth, Coalescence, and the Size Distribution of Droplets". In: *Phys. Rev. Lett.* 109 (6 2012), p. 068701. DOI: 10.1103/PhysRevLett.109.068701. URL: http://link.aps.org/doi/10.1103/PhysRevLett.109.068701.

[4]   Hua Dong et al. "Bioinspired electrospun knotted microfibers for fog harvesting". In: *ChemPhysChem* 13.5 (2012), pp. 1153–1156.

[5]   Fereydoon Family and Paul Meakin. "Kinetics of droplet growth processes: Simulations, theory, and experiments". In: *Physical Review A* 40.7 (1989), p. 3836.

[6]   Gunnar Klös. "Time evolution of the size distribution of droplets on a string". Bachelor's Thesis. Georg-August-Universität Göttingen, 2013.

[7]   Otto Klemm et al. "Fog as a fresh-water resource: overview and perspectives". In: *Ambio* 41.3 (2012), pp. 221–234.

[8]   Tobias Lapp. "Evolution of Droplet Distributions in Hydrodynamic Systems". Dissertation. Georg-August-Universität Göttingen, 2011.

[9]   Lord Rayleigh. "Breath figures". In: *Nature* 86.2169 (1911), pp. 416–417.

[10] H Saleur, CG Sammis, and D Sornette. "Discrete scale invariance, complex fractal dimensions, and log-periodic fluctuations in seismicity". In: *Journal of Geophysical Research: Solid Earth (1978–2012)* 101.B8 (1996), pp. 17661–17677.

[11] Basant Singh Sikarwar et al. "Dropwise condensation studies on multiple scales". In: *Heat Transfer Engineering* 33.4-5 (2012), pp. 301–341.

[12] Didier Sornette. "Discrete-scale invariance and complex dimensions". In: *Physics reports* 297.5 (1998), pp. 239–270.

[13] AL Yarin et al. "Liquid drop growth on a fiber". In: *AIChE Journal* 52.1 (2006), pp. 217–227.

Erklärung nach §13(8) der Prüfungsordnung für den Bachelor-Studiengang Physik und den Master-Studiengang Physik an der Universität Göttingen:

Hiermit erkläre ich, dass ich diese Abschlussarbeit selbständig verfasst habe, keine anderen als die angegebenen Quellen und Hilfsmittel benutzt habe und alle Stellen, die wörtlich oder sinngemäß aus veröffentlichten Schriften entnommen wurden, als solche kenntlich gemacht habe.

Darüberhinaus erkläre ich, dass diese Abschlussarbeit nicht, auch nicht auszugsweise, im Rahmen einer nichtbestandenen Prüfung an dieser oder einer anderen Hochschule eingereicht wurde.

Göttingen, den 23. Oktober 2014

(Philipp Dönges)